Elastic-Plastic Dynamic Buckling of Thin-Shell Finite Elements with Asymmetric Imperfections

T. Y. Yang* and D. G. Liaw†
Purdue University, West Lafayette, Indiana

In an earlier study of the phenomena of dynamic buckling of shells in the elastic range using a 48 degree-of-freedom doubly curved quadrilateral imperfect thin-shell finite element, the interesting destabilizing effects of initial imperfections on a spherical shell, a spherical cap, and a hemispherical shell were found. The formulation was based on the Kirchhoff-Love shell theory with geometric imperfections. In this study, the earlier formulation is extended to include the effect of plasticity in tensor form so that a wide range of practical problems can be considered in order to study more completely the effects of dynamics, amplitude of imperfection, and plasticity. The effect of viscous damping is also considered by using the Rayleigh damping concept. Examples include static and dynamic buckling analyses of 1) axisymmetrically imperfect spherical shells, 2) axisymmetrically imperfect spherical caps, and 3) asymmetrically imperfect spherical caps, all in both elastic and elastic-plastic ranges. For case 3, there seems to be no previous results available for comparison. From the wide variety of examples studied, the previous conclusions for shells with axisymmetric imperfections were reconfirmed for shells with asymmetric imperfections, i.e., dynamic effect, imperfection, and plastic deformation, which all have the effect of reducing the buckling load to various degrees. On the contrary, the viscous damping has the effect of increasing the dynamic buckling load. Such an effect is quantified in two examples.

Introduction

THIN shells are a popular and useful form of structural components, with many significant applications in engineering. However, the stability behavior of thin shells is usually very sensitive to the initial imperfections that are often induced due to the difficulty in achieving manufacturing accuracy. Thus, the studies of the effects of initial imperfections on the stability behavior of thin shells have attracted considerable attention. A review of such efforts can be found, for example, in the text by Bushnell[1] and the review paper by Jones.[2] The studies of static buckling were too numerous to be referenced. In this section, only a very limited number of references are mentioned. A formulation for a general theory to study the influence of initial geometric imperfections on the buckling load of shells was due to Koiter.[3]

Cylindrical shells with general imperfect shapes containing both axisymmetric and asymmetric components were studied by Hutchinson.[4] In addition to shells of cylindrical shape, many investigators also studied the influence of imperfections on the buckling pressures of shells with shapes of complete sphere[5] and spherical cap.[6] All of these studies were based on the solutions of differential equations using an analytical approach. In parallel, numerical methods were also employed. For example, Huang[7] used the finite-difference method to study the unsymmetric buckling of spherical shells. Kao and Perrone[8] and Kao[9] used the finite-difference method to study the spherical cap under asymmetric imperfections. Kao[10] continued his work to study elastic-plastic buckling under axisymmetric imperfections. Tong and Pian[11] formulated and used a revolutional-shell finite element to study the postbuckling behavior of shells of revolution. Kapania and Yang[12] formulated a quadrilateral doubly curved thin-shell finite element to study the postbuckling behavior of general shell structures.

Studies of dynamic buckling were also too numerous to be referenced completely. A brief review was given in Ref. 13, which will not be repeated here. Only several key references, which provided examples and numerical results pertinent to the examples studied here, are mentioned. These include: the studies of elastic dynamic axisymmetrical buckling of clamped spherical caps by Budiansky and Roth[14] using the Rayleigh-Ritz method and also by Huang[15] using the finite-difference approach; the study of asymmetrical elastic buckling of cylindrical and spherical shells using revolutional-shell finite elements by Stricklin et al.[16]; the studies of elastic[17] and elastic-plastic[18] dynamic buckling of spherical caps by Kao and Perrone using the finite-difference method; and the study of elastic-plastic dynamic buckling of spherical shells by Ishizaki and Bathe[19] using axisymmetrical solid elements with 8-node quadrilateral cross sections.

Because of the universality of using finite elements in modeling shells with complex loadings, arbitrary geometries, and realistic boundary conditions, the finite-element methods appear attractive in solving dynamic buckling problems of shell structures with practical design. In an earlier study, Saigal et al.[13] studied the phenomena of dynamic buckling of shells in the elastic range using 48 degree-of-freedom doubly curved quadrilateral imperfect thin-shell element. In the formulation, the middle surface of the shells and the geometric imperfections were specified using variable-order polynomials so as to allow representation of a wide range of shell geometries and imperfections. These variable-order polynomials were different from the displacement functions. The formulation was based on the Kirchhoff-Love shell theory. The geometric imperfections were treated by including additional terms in the strain-displacement equations, which were extended from the relation given by Niordson[20] for perfect shells.

It is the intent of this study to extend this earlier formulation to include the effects of plasticity in tensor form and viscous damping by using the Rayleigh damping concept[21] so that a wide range of problems can be studied. In the plastic range, the Prandtl-Reuss flow theory and the von Mises yield criterion are used, and the spread of plastic zones in the thickness direction is treated by using a layered-element method.

Received March 12, 1987.

*Professor of Aeronautics and Astronautics and Dean of Engineering. Fellow AIAA.

†Graduate Research Assistant, School of Aeronautics and Astronautics.

The examples studied here include the static and dynamic buckling analyses of 1) axisymmetrically imperfect spherical shells, 2) axisymmetrically imperfect spherical caps, 3) asymmetrically imperfect spherical caps, all in both elastic and elastic-plastic ranges. For case 3, there seems to be no previous results available for comparison.

From the wide variety of examples studied, the previous conclusions for shells with axisymmetrical imperfections were reconfirmed for shells with asymmetrical imperfections, i.e., dynamic effect, imperfection, and plastic deformation, which all have the effect of reducing the buckling load. On the contrary, viscous damping has the effect of increasing the dynamic buckling load. Such an effect is quantified in two examples.

Formulation

The shell element was developed by the senior author and his coworkers to the extent that it can treat elastic imperfect shells[12,13] and inelastic perfect shells.[22] The formulation is extended here to include the combined effects of imperfection and inelasticity.

Strain-Displacement Relations

The strain-displacement relations for imperfect shells are represented in terms of Cartesian components and are an extended version of the strain-displacement relations given in tensor form by Niordson.[20] The effects of imperfections are included by modifying the tangential strain-displacement relations. These are given as

$$e_{\alpha\beta} = \tfrac{1}{2}(f,^{i}_{\alpha}u,^{i}_{\beta} + f,^{i}_{\beta}u,^{i}_{\alpha} + u,^{i}_{\alpha}u,^{i}_{\beta} + v,^{i}_{\alpha}u,^{i}_{\beta} + u,^{i}_{\alpha}v,^{i}_{\beta}) \tag{1}$$

where f^i, u^i, and v^i are the Cartesian components of the middle surface, displacement, and imperfection at a given point on the shell surface, respectively; i varies from 1 to 3 and α and β from 1 to 2. In this study, the effects of imperfections on the curvature-displacement relations are ignored.

Stress-Strain Relations

The material considered is elastic-plastic with or without strain hardening. A general stress-strain relation can be written as

$$\{\Sigma\} = [D]\{E\} \tag{2}$$

In the elastic range, constitutive equations can be given as

$$N^{\alpha\beta} = H^{\alpha\beta\lambda\mu} e_{\lambda\mu} \tag{3}$$

and

$$M^{\alpha\beta} = \frac{h^2}{12} H^{\alpha\beta\lambda\mu} k_{\lambda\mu} \tag{4}$$

where $N^{\alpha\beta}$ is the in-plane stress resultant tensor, $M^{\alpha\beta}$ the stress couple tensor, $e_{\lambda\mu}$ the tangential strain tensor, $k_{\lambda\mu}$ the curvature tensor, and $H^{\alpha\beta\lambda\mu}$ the tensor of elastic moduli in the form

$$H^{\alpha\beta\lambda\mu} = \frac{Eh}{2(1+\nu)}\left[a^{\alpha\lambda}a^{\beta\mu} + a^{\alpha\mu}a^{\beta\lambda} + \frac{2\nu}{1-\nu}a^{\alpha\beta}a^{\lambda\mu}\right] \tag{5}$$

where E is Young's modulus, ν Poisson's ratio and, $a^{\alpha\beta}$ the contravariant component of the metric tensor, which is related to $a_{\alpha\beta}$ through the relation

$$a^{\alpha\beta}a_{\alpha\beta} = \delta^{\alpha}_{\beta} \tag{6}$$

with δ^{α}_{β} being the Kronecker symbol. Equations (3) and (4) can be rearranged in the following matrix form:

$$\{\Sigma\} = \begin{Bmatrix} N \\ M \end{Bmatrix} = \begin{bmatrix} D^e_m & 0 \\ 0 & D^e_b \end{bmatrix} \begin{Bmatrix} e \\ k \end{Bmatrix} = [D^e]\{E\} \tag{7}$$

where $D^e_b = (h^2/12)D^e_m$.

In the plastic range, the total increments in strain are assumed to be separated into elastic and plastic components given as

$$d\{\epsilon\} = d\{\epsilon^e\} + d\{\epsilon^p\} \tag{8}$$

The general equations for yield surface and plastic potential are given, respectively, in symbolic forms as

$$F(\{\sigma\},K) = 0 \tag{9}$$

and

$$Q(\{\sigma\},K) = 0 \tag{10}$$

where K is a hardening parameter, $\{\epsilon\}$ the strain vector, and $\{\sigma\}$ the stress vector.

It is important to note that, for simplicity of formulation, all strains and stresses are derived in tensor form as given in Eqs. (3, 4). However, when determining the plastic zones, the strains and stresses must be converted from tensor components to physical components given as

$$\sigma_{\alpha\beta} = a_{\alpha\beta}N^{\alpha\beta} \tag{11}$$

and

$$\epsilon_{\alpha\beta} = a_{\alpha\beta}e^{\alpha\beta} \tag{12}$$

so that their physical quantities can be identified. It is further noted that including the geometric imperfections in tensor form as in the strain-displacement equation (1) and subsequently converting the strains and stresses into physical components in Eqs. (11) and (12), which contain the effect of imperfections, are the key steps in simultaneously accounting for the combined effects of both imperfection and plasticity.

The elatic strains associated with plasticity are obtained from Eqs. (7), (11), and (12) as

$$d\{\epsilon^e\} = [D^e_m]^{-1}d\{\sigma\} \tag{13}$$

For plastic strains, the normality rule requires that

$$d\{\epsilon^p\} = d\lambda\{a^*\} \tag{14}$$

where $\{a^*\} = \partial Q/\partial\{\sigma\}$, and $d\lambda$ is a positive proportionality constant.

During plastic deformation, the stresses remain on the yield surface so that

$$dF = \{a\}^T d\{\sigma\} - A\,d\lambda = 0 \tag{15}$$

where

$$\{a\} = \frac{\partial F}{\partial}\{Q\},$$

and the scalar

$$A = \left(\frac{-1}{d\lambda}\right)\left(\frac{\partial F}{\partial K}\right)dK$$

For associative plasticity, $\{a\} = \{a^*\}$. If the yield surface is defined in terms of a uniaxial stress, the scalar A is equal to the slope S of the uniaxial stress-plastic strain curve

$$A = S = \frac{E_T}{1 - E_T/E} \tag{16}$$

Substituting Eqs. (13) and (14) into Eq. (8) gives

$$d\{\epsilon\} = [D_m^e]^{-1} d\{\sigma\} + d\lambda\{a^*\} \tag{17}$$

Premultiplying Eq. (17) by $\{a\}^T[D_m^e]$ and eliminating $d\{\sigma\}$ gives

$$\{a\}^T[D_m^e]d\{\epsilon\} = A d\lambda + \{a\}^T[D_m^e]\{a^*\}d\lambda \tag{18}$$

Solving $d\lambda$ from Eq. (18) and substituting $d\lambda$ into Eq. (17) gives

$$d\{\sigma\} = [D_m^p]d\{\epsilon\} \tag{19}$$

where

$$[D_m^p] = [D_m^e] - \frac{[D_m^e]\{a^*\}\{a\}^T[D_m^e]}{A + \{a\}^T[D_m^e]\{a^*\}}$$

The stress-strain relations in the plastic range are finally obtained in matrix form

$$\{\Sigma\} = \begin{Bmatrix} N \\ M \end{Bmatrix} = \begin{bmatrix} D_m^p & 0 \\ 0 & D_b^p \end{bmatrix} \begin{Bmatrix} e \\ k \end{Bmatrix} = [D^p]\{E\} \tag{20}$$

where $D_b^p = (h^2/12)D_m^p$. Equation (20) is consistent with Eq. (7) in the elastic range. Such consistency has the effect of simplifying the computational and programming procedures. (The preceding notations follow those of Refs. 22–24.)

Solution Procedures

The nonlinear equations of motion are solved by an incremental procedure combined with iterative techniques for equilibrium. Newmark's generalized operator for numerical integration is used in the dynamic analysis. To achieve equilibrium at the new state, the modified Newton-Raphson iterative procedure is performed for each incremental step to keep the unbalanced forces and incremental displacements within the specified convergence criteria:

$$\left[\left(\sum_{i=1}^{N} \Delta P_i^2\right) \Big/ \left(\sum_{i=1}^{N} P_i^2\right)\right]^{1/2} \le 0.01\%$$

$$\left[\left(\sum_{i=1}^{N} \Delta q_i^2\right) \Big/ \left(\sum_{i=1}^{N} q_i^2\right)\right]^{1/2} \le 0.01\% \tag{21}$$

where the subscript i is the degree-of-freedom number, N the total number of degrees of freedom of the finite-element modeling, ΔP_i the unbalanced force between the applied load and the internal force, P_i the current applied load, Δq_i the incremental displacement, and q_i the current displacement.

Results

The elastic version of the present finite-element formulations and the solution procedures have been applied for static[12] and dynamic[13] shell-buckling analyses with geometric nonlinearity and initial imperfections. Additional effort to include the initial imperfections in strain-displacement equation (1) in tensor form and also to convert the strains and stresses from tensor components to vector components using Eqs. (11) and (12) has enabled this study to cover a wide range of dynamic buckling problems of shells with the simultaneous effect of inelasticity and imperfections.

It is of interest to consider the effect of damping on the dynamic characteristics of buckling. The simple assumption for viscous damping using a Rayleigh damping concept[21] was used. The explicit viscous damping matrix was obtained by the proportional sum of the consistent mass and stiffness matrices. Two fundamental frequencies (ω_1 and ω_2) were obtained to evaluate the two proportionality factors a and b:

$$2\xi_1\omega_1 = a + b\omega_1^2$$

$$2\xi_2\omega_2 = a + b\omega_2^2 \tag{22}$$

where the modal damping ratios ξ_1 and ξ_2 were both assumed as 5% in this study.

This study includes: 1) dynamic buckling analysis of a complete spherical shell with material nonlinearity and axisymmetric imperfections, 2) static and dynamic buckling analysis of a spherical cap with material nonlinearity and axisymmetric imperfections, and 3) static and dynamic buckling analysis of a spherical cap with material nonlinearity and asymmetric imperfections. These three examples cover eight cases, as categorized in Table 1. for the first five cases, alternative numerical solutions are available for evaluation of the present formulations and computer program. The last three cases provide new results.

In all the examples studied, the shell element was divided into eight layers, within each layer a 5×5 Gauss grid was used to evaluate all of the integrals. All calculations were performed using a CYBER 205 vectorized supercomputer at Purdue University.

1) Dynamic Buckling Analysis of a Complete Spherical Shell with Material Nonlinearity and Axisymmetric Imperfections (Case 4 in Table 1).

The dynamic buckling analysis for a complete spherical shell with initial axisymmetric imperfections under step uniform pressure with infinite duration was first studied. The spherical shell has a thickness of 1 in. and a radius of 100 in. The material was assumed as 6061-T6 aluminum with the following properties: $E = 1.0\times10^7$ psi; $\nu = 1/3$; $\sigma_y = 4.1\times10^4$ psi; $E_T = 2.0\times10^5$ psi; $\rho = 0.254\times10^{-3}$ lb-s/in.[4]

Due to axisymmetry, a strip of the sphere subtending an angle of 10 deg in the circumferential direction and 90 deg in the meridional direction was analyzed using six elements (a total of 48 unconstrained degrees of freedom) graded as

Table 1 Eight cases studied in the present three examples and the related references

	Elastic		Elastic-plastic	
	Static	Dynamic	Static	Dynamic
Axisymmetric imperfections	(1)[a] Kao[10] Kapania and Yang[12] This study	(2) Kao and Perrone[17] Saigal et al.[13] This study	(3) Kao[10] This study	(4) Kao[18] Ishizaki and Bathe[19] This study
Asymmetric imperfections	(5) Kao and Perrone[8,9] This study	(6) This study	(7) This study	(8) This study

[a]Case number

shown in Fig. 1. The imperfections considered were of the following axisymmetric form:

$$W_0(\phi) = \delta h P_{18}(\cos\phi)$$

where ϕ is the meridional angle measured from the pole of the sphere, δ the amplitude of imperfection, h the thickness of the shell, and $P_{18}(\cos\phi)$ the Legendre polynomial of order 18.

The time variable t was nondimensionalized as

$$\tau = \sqrt{(E/\rho R^2)}\,t$$

It was found that when the time increment $\Delta\tau$ was reduced to 0.2, the dynamic response curves became convergent. For example, results for $\Delta\tau = 0.05$ were found to be no different than those for $\Delta\tau = 0.2$.

To determine the dynamic buckling load is tedious because the transient responses must be calculated for an appropriate range of loads. This process is demonstrated for a perfect spherical shell, with results shown in Fig. 1 where the mean displacement was plotted against nondimensional time τ for four values of step uniform pressure: $P = 0.60P_{cr}$ $0.62P_{cr}$, $0.63P_{cr}$, and $0.65P_{cr}$. The symbol P_{cr} is the classical axisymmetric static buckling load of the complete spehrical shell, given as

$$P_{cr} = 2E/[3(1-\nu^2)]^{1/2}(h/R)^2$$

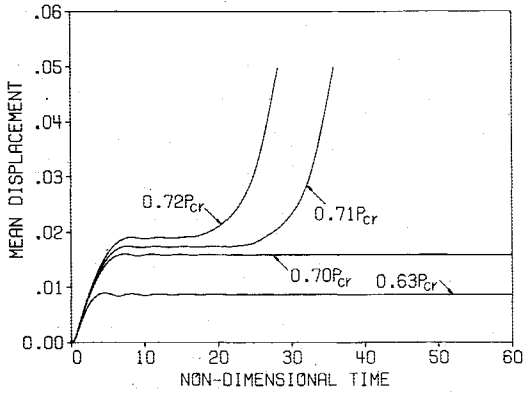

Fig. 1 Elastic-plastic dynamic response of a perfect complete spherical shell under uniform step pressure.

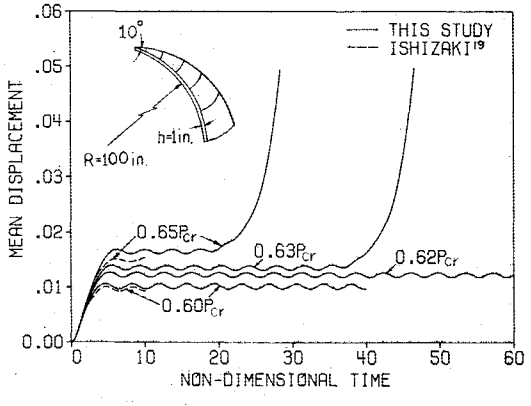

Fig. 2 Elastic-plastic damped responses of a perfect complete spherical shell under uniform step pressures (modal damping ratios $\xi_1 = \xi_2 = 0.05$).

Mean displacement was defined by previous researchers as

$$\frac{\text{Volume change due to shell deformation}}{\text{Original volume within the shell}}$$

This problem was considered by Ishizaki and Bathe[19] using 20 axisymmetric solid elements with 8-node quadrilateral cross sections to model half of the spherical shell. The modeling constituted a total of 200 unconstrained degrees of freedom. Their results are also plotted in Fig. 2 as dashed curves.

It is seen that the response curve for $P = 0.63P_{cr}$ exhibits a pronounced increase after $\tau = 36$, whereas the response curve for $P = 0.62P_{cr}$ remains steady. Thus, it can be estimated that the dynamic buckling load lies between $0.62P_{cr}$ and $0.63P_{cr}$. Alternatively, whether the response curve is steady or not can be found by comparing its peak or valley values at each cycle with the previous cycle. Figure 1 not only provides for the information for estimation of the dynamic buckling load, but also gives some clear time-history information for the responses under various loadings.

The response of the perfect spherical shell due to the aforementioned effect of viscous damping are shown in Fig. 2. When comparing the results of Figs. 1 and 2, it is observed that the assumed viscous damping based on two fundamental modal damping ratios of 5% has the effect of increasing the dynamic buckling load by approximately 10%.

Based on the procedure for searching for the dynamic buckling load for the perfect spherical shell shown in Fig. 1, results were obtained for imperfect shells with three different amplitude values ($\delta = 0.1$, 0.2, and 0.4). The present values are bracketed with those upper and lower estimated values by Ishizaki and Bathe.[20] Figure 3 shows that the amplitude

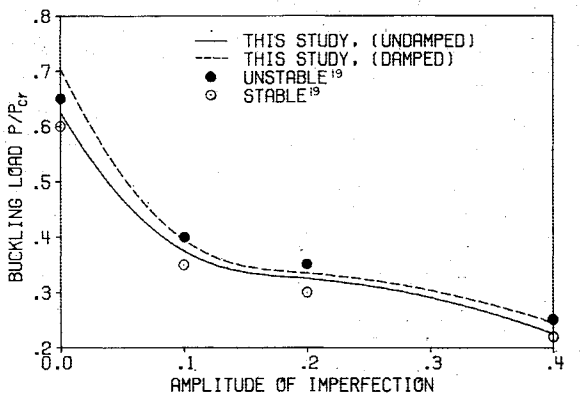

Fig. 3 Elastic-plastic dynamic buckling analysis of a complete spherical shell with axisymmetric imperfections.

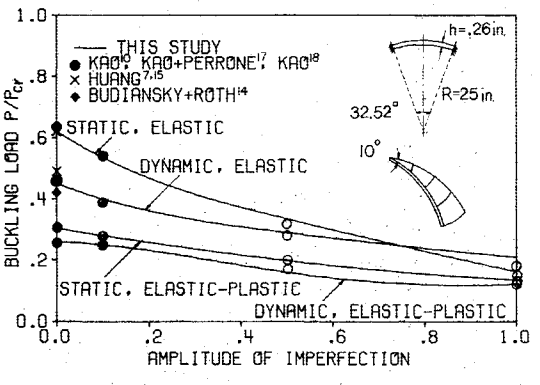

Fig. 4 Static and dynamic buckling analyses of a spherical cap ($\lambda = 5$) with axisymmetric initial imperfections.

of imperfection has a significant effect in reducing the dynamic buckling load. When the amplitude becomes 40% of the thickness, the dynamic buckling load is reduced to 22% of its classically axisymmetric buckling value. The results due to the effect of viscous damping with $\xi_1 = \xi_2 = 5\%$ are also shown in Fig. 3. As a result, the dynamic buckling loads are, in general, increased by approximately 5 ~ 10%.

2) Static and Dynamic Buckling Analysis of a Spherical Cap with Material Nonlinearity and Axisymmetric Imperfections (Cases 1-4 in Table 1).

The geometry of the spherical cap was defined by setting the geometric parameter λ as 5, which is defined as

$$\lambda = 2[3(1-\nu^2)]^{1/4}(H/h)^{1/2}$$

with H defined as the rise of the middle surface at the apex of the shell. The spherical cap was assumed as clamped with thickness $h = 0.26$ in., radius $R = 25$ in., and a subtending angle of 32.52 deg, as shown in Fig. 4. The geometry of the axisymmetric imperfection was defined as

$$W_0(\phi) = \delta h[1 - (25 \sin\phi/7)^2]^3$$

Due to axisymmetry, only a 10 deg segment was analyzed using four elements with equal meridional subtending angles, as shown in Fig. 4.

The material properties were assumed as to be $E = 3.0 \times 10^7$ psi, $\nu = 0.3$, $\sigma_y = 6.0 \times 10^4$ psi, $E_\tau = 3.0 \times 10^6$ psi, and $\rho = 0.254 \times 10^{-3}$ lb-s^2/in.^{4}.

In both static and dynamic buckling analyses, the loadings were assumed to be uniformly distributed. For dynamic analysis, the pressure was assumed to be a step function. The time increment of $\Delta\tau = 0.25$ was used to obtain all results. It was further verified that when $\Delta\tau$ was refined as 0.1, the response curves remain the same as those obtained using $\Delta\tau = 0.25$.

For this example, results were obtained as shown in Fig. 4 for four cases: a) static and elastic, b) dynamic and elastic, c) static and elastic-plastic, and d) dynamic and elastic-plastic.

This problem was studied previously by several investigators, and their results are also plotted in Fig. 4 for comparison. Kao,[10,18] and Kao and Perrone,[17] used the finite-difference method to form sets of nonlinear algebraic equations and obtained solutions using a nonlinear relaxation technique. Huang used the finite-difference approach to solve the elastic-static unsymmetric buckling problem[7] and the elastic dynamic axisymmetric buckling problem[15] for the case of a perfect shell. For the case of static unsymmetric buckling, the buckling mode becomes symmetric for the present value of $\lambda = 5$. The value obtained by Huang were 0.629 for the static buckling load and 0.49 for the dynamic buckling load.

Alternatively, Budiansky and Roth[14] used the Rayleigh-Ritz method with five terms to solve the elastic dynamic buckling problem of a perfect shell. The dynamic buckling load obtained in Ref. 14 is 0.42. As can be seen, all of the results obtained from these six references are in good agreement with the present results, with the exceptions of the elastic dynamic buckling load for the perfect shell of 0.49 obtained by Huang,[15] which is 9% higher than the value of 0.45 of this study, and of 0.42 obtained by Budiansky and Roth, which is 7% lower than the present value.

3) Static and Dynamic Buckling Analysis of a Spherical Cap with Material Nonlinearity and Asymmetric Imperfections (Cases 5-8 in Table 1).

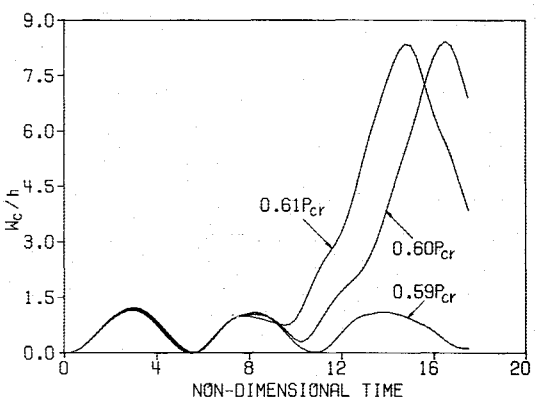

Fig. 6 Elastic dynamic response of a perfect spherical cap ($\lambda = 6$) under uniform step pressures.

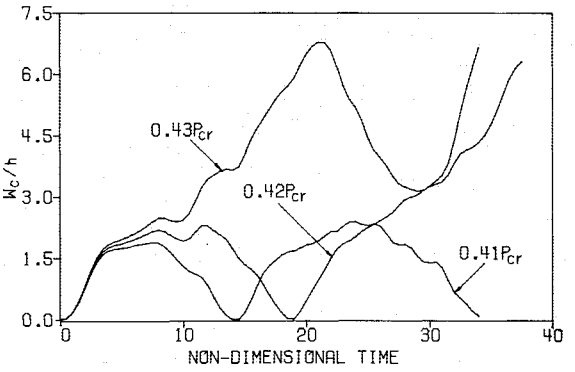

Fig. 7 Elastic dynamic response of an imperfect ($\delta = 0.4$) spherical cap ($\lambda = 6$) with asymmetric imperfections.

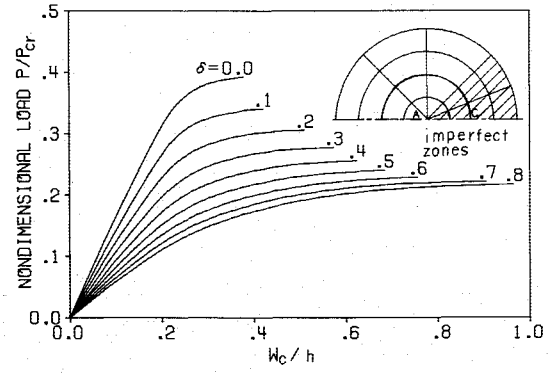

Fig. 5 Elastic-plastic static buckling analysis of a spherical cap ($\lambda = 6$) with asymmetric imperfections.

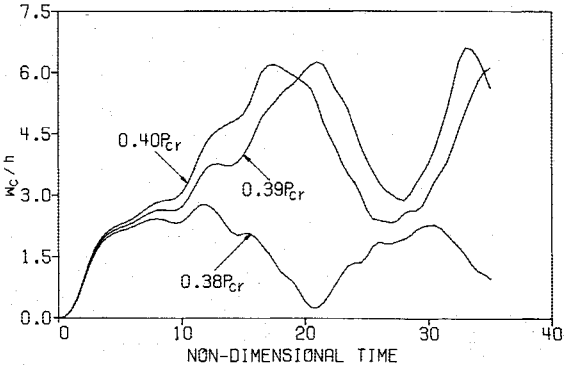

Fig. 8 Elastic dynamic response of an imperfect ($\delta = 0.8$) spherical cap ($\lambda = 6$) with asymmetric imperfections.

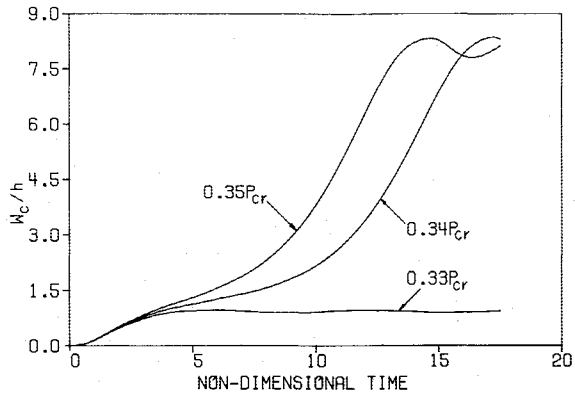

Fig. 9 Elastic-plastic dynamic response of a perfect spherical cap ($\lambda = 6$) under uniform step pressure.

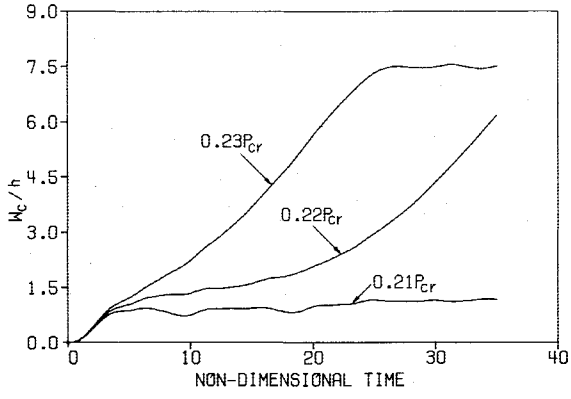

Fig. 10 Elastic-plastic dynamic response of an imperfect ($\delta = 0.4$) spherical cap ($\lambda = 6$) with asymmetric imperfections.

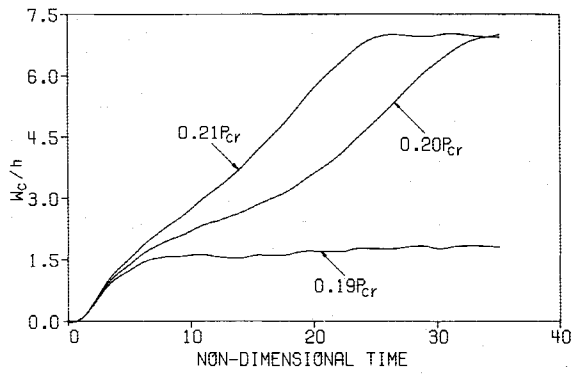

Fig. 11 Elastic-plastic dynamic response of an imperfect ($\delta = 0.8$) spherical cap ($\lambda = 6$) with asymmetric imperfections.

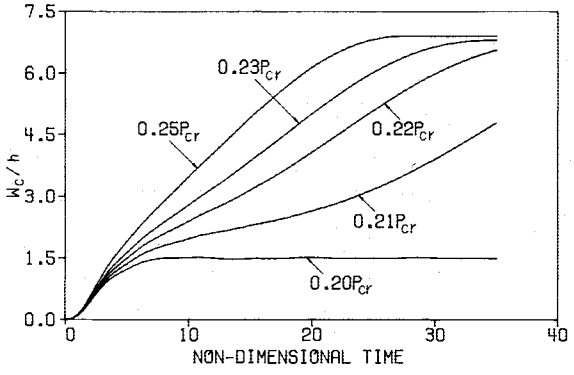

Fig. 12 Elastic-plastic damping response of an imperfect ($\delta = 0.8$) spherical cap ($\lambda = 6$) with asymmetric imperfections (modal damping ratios $\xi_1 = \xi_2 = 0.05$).

For this spherical cap, the geometric parameter λ was assumed to be 6. The thickness h and radius R were assumed as 0.1778 and 25 in., respectively. The boundary was assumed to be clamped.

The imperfection was assumed asymmetric, which was confined within the shape of a cut pie, as shown in the shaded zone in Fig. 5. The imperfection was defined as

$$W_0(\phi,\theta) = 64\delta h\left(\frac{25}{7}\sin\phi\right)^3\left(1-\frac{25}{7}\sin\phi\right)^3\cos 2\theta$$

In this study, the imperfection zone was assumed to be confined within a quadrant of the spherical cap, i.e., $|\theta| \le 45$ deg.

The material properties of this shell were assumed to be the same as those of the example 2. The shell was modeled using 20 elements (Fig. 5) among which eight were used to model the imperfect zone. This mesh was shown to be sufficiently fine, as an alternative finer mesh (54 elements and 634 unconstrained degrees of freedom) was used and the results were essentially the same as those obtained using the 20-element mesh. The nondimensional time increment was $\Delta\tau = 0.25$, which was shown to be sufficiently fine by using another $\Delta\tau$ of 0.1.

Figure 5 shows the results of elastic-plastic static buckling of the spherical cap with various amplitudes of asymmetric imperfections ($\delta = 0, 0.1, \ldots, 0.8$). The effect of amplitude on the static buckling load is apparent; the same as that observed in the axisymmetrically imperfect case.

Figures 6, 7, and 8 show the results for the elastic dynamic responses of the spherical cap with three different amplitudes of asymmetric imperfections, i.e., $\delta = 0$, 0.4, and 0.8, respectively. Figure 6 shows the interesting phenomenon of dynamic buckling as the uniform step pressure increased by a small amount from $0.59P_{cr}$ to $0.60P_{cr}$. Figure 7 shows that, for the case of an imperfect shell with $\delta = 0.4$, the dynamic response became more irregular than that for the perfect shell. It is observed that the dynamic buckling load was reduced to between $0.41P_{cr}$ and $0.42P_{cr}$. Figure 8 shows that, for $\delta = 0.8$, the dynamic buckling load was further reduced to between $0.38P_{cr}$ and $0.39P_{cr}$. The reduction of dynamic buckling load from the case of $\delta = 0$ to 0.4 appears much more pronounced than that form the case of $\delta = 0.4$ to 0.8.

Figures 9, 10, and 11 show the results for the elastic-plastic dynamic responses of the spherical cap with three different amplitudes of asymmetric imperfections, i.e., $\delta = 0$, 0.4, and 0.8, respectively. Figure 9 shows the obvious dynamic buckling effect when the uniform step pressure was slightly increased from $0.33P_{cr}$ to $0.34P_{cr}$ for the case of a perfect shell ($\delta = 0$). Figure 10 shows that when $\delta = 0.4$, the dynamic buckling was reduced to between $0.21P_{cr}$ and $0.22P_{cr}$. Figure 11 shows that when $\delta = 0.8$, the dynamic buckling load was further reduced slightly to between $0.19P_{cr}$ and $0.20P_{cr}$. Again, it is observed that the reduction of dynamic buckling load due to the increase in amplitude of asymmetric imperfection is far more pronounced in the former case (from $\delta = 0.0$ to 0.4) than the latter case (from $\delta = 0.4$ to 0.8).

The responses of the imperfect spherical cap with $\delta = 0.8$ due to the aforementioned effect of viscous damping are shown in Fig. 12. When comparing the results of Figs. 11 and 12, it is observed that the assumed viscous damping based on two fundamental modal damping ratios of 5% has the effect of increasing the dynamic buckling load by approximately 5%.

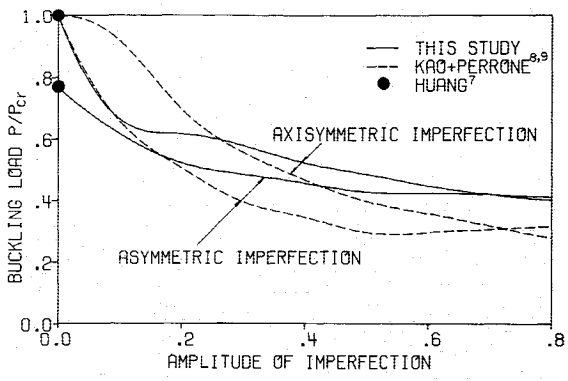

Fig. 13 Elastic static buckling analyses of spherical cap ($\lambda = 6$) with initial imperfections.

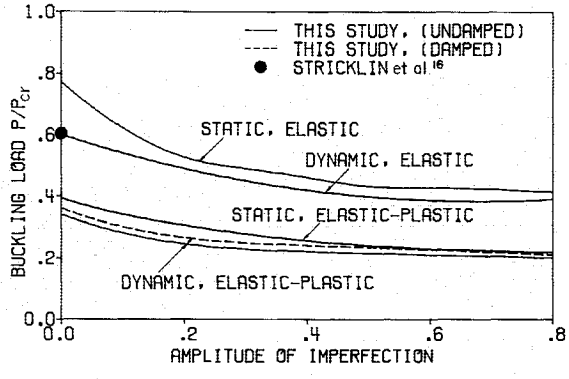

Fig. 14 Static and dynamic buckling analyses of a spherical cap ($\lambda = 6$) with asymmetric initial imperfections.

Figure 13 shows the results for elastic and static buckling loads of the spherical cap with both types of imperfections, axisymmetric and asymmetric, respectively. This example was analyzed by Kao and Perrone[8,9] previously, and their results were also plotted as two curves in Fig. 13. The general trend of buckling load against amplitude of imperfection for both sets of curves appears to be similar, and also the magnitudes of those curves are not too far apart.

This problem was also treated by Huang[7] as an eigenvalue problem to find the aysmmetric buckling pressure for a perfect shell ($\delta = 0$) within a wide range of geometric parameters. For $\lambda = 6$, he found the static buckling loads to be $0.775P_{cr}$ and $0.995P_{cr}$ for the asymmetrical and axisymmetrical modes, respectively. These two values are very close to the present two values of $0.77P_{cr}$ and $1.0P_{cr}$, respectively. Huang's two values were also plotted in Fig. 13. They seem to validate the present results for the case of $\delta = 0$.

Figure 14 shows the results for the present spherical cap with symmetric imperfection for four cases: a) static and elastic, b) dynamic and elastic, c) static and elastic-plastic, d) dynamic and elastic-plastic. The results due to the effect of viscous damping with $\xi_1 = \xi_2 = 5\%$ are also shown in Fig. 14. As a result, the dynamic buckling loads are, in general, increased by approximately $5 \sim 10\%$. It is interesting to see that as the δ value increases beyond, say, 0.5, the effect of δ on the reduction of buckling load becomes much less pronounced For the special case of the elastic perfect shell ($\delta = 0$), Stricklin et al.[16] obtained a dynamic buckling load of $0.604P_{cr}$ using axisymmetrical shell finite elements. The value was plotted in Fig. 14, which is very close to the present value of $0.60P_{cr}$.

Concluding Remarks

In this study, an earlier formulation for a 48 degree-of-freedom doubly curved thin elastic shell finite element with imperfection and that for the same element without imperfection but with plastic effect were extended to include the combined effects of plasticity and geometric imperfection. The geometric imperfection was included in the strain-displacement equations in tensor form, and the stress-strain equations were eventually converted to physical components so that physical quantities of stresses and strains can be obtained to identify the plastic boundaries.

The validity of the present formulation is established through comparison of the present results with a series of examples, as systematically tabulated in Table 1. New results were also obtained to provide insight into the dynamic elastic and elastic-plastic buckling of spherical caps with axisymmetric and asymmetric imperfections.

The present results for the spherical caps show that the dynamics, plastic deformation, and imperfection will have the effect of reducing the buckling load for the case of axisymmetric as well as asymmetric imperfections. However, the present example (3 above) indicates that the effect of amplitude (δ) of asymmetric imperfection on the reduction of buckling load is more pronounced, as δ is relatively smaller.

The effect of viscous damping was studied using the simple Rayleigh damping assumption based on two modal damping ratios only with $\xi_1 = \xi_2 = 5\%$. For the two specific examples studied, it was indicated that the dynamic buckling loads were, in general, increased by about $5 \sim 10\%$.

Acknowledgments

This study was sponsored by the National Science Foundation through Grant ECE-8516915. Technical guidance from M. P. Gaus, S. C. Liu, and C. Astill is acknowledged. The computer program was primarily developed by R. K. Kapania, S. Saigal, and the senior author. The work done by Messrs. Kapania and Saigal is also acknowledged.

References

[1]Bushnell, D., *Computerized Buckling Analysis of Shells*, Martinus Nijhoff Publishers, Dordrecht, the Netherlands, 1985.

[2]Jone, N., "Dynamic Elstic and Inelastic Buckling of Shells," *Developments in Thin-Walled Structures-2*, edited by J. Rhodes and A. C. Walker, Elsevier, England, 1984, pp. 49–91.

[3]Koiter, W. T., "Over de Stabiliteit van het elastic evenwicht," Delft University thesis, H. T. Paris, Amsterdam, 1945 (English translation, NASA Rept. TT F-10, 1967).

[4]Hutchinson, J. W., "Axial Buckling of Pressurized Imperfect Cylindrical Shell," *AIAA Journal*, Vol. 3, Aug. 1965, pp. 1461–1466.

[5]Walker, A. C., "An Analytical Study of the Rotationally Symmetric Nonlinear Buckling of a Complete Spherical Shell Under External Pressure," *International Journal of Mechanical Sciences*, Vol. 10, Sept. 1968, pp. 695–710.

[6]Hutchinson, J. W., "Imperfection-Sensitivity of Externally Pressurized Spherical Shells," *Journal of Applied Mechanics*, Vol. 34, March 1967, pp. 49–55.

[7]Huang, N. C., "Unsymmetrical Buckling of Thin Shallow Spherical Shells," *Journal of Applied Mechanics*, Vol. 31, Sept. 1964, pp. 447–457.

[8]Kao, R. and Perrone, N., "Asymmetric Buckling of Spherical Caps with Asymmetrical Imperfections," *Journal of Applied Mechanics*, Vol. 38, March 1971, pp. 172–178.

[9]Kao, R., "A Note on Buckling of Spherical Caps with Initial Asymmetric Imperfections," *Journal of Applied Mechanics*, Vol. 39, Sept. 1972, pp. 842–844.

[10]Kao, R., "Large Deformation Elastic-Plastic Buckling Analysis of Spherical Caps with Initial Imperfections," *Computers and Structures*, Vol. 11, 1980, pp. 609–619.

[11]Tong, P. and Pian, T. H. H., "Postbuckling Analysis of Shells of Revolution by the Finite Element Method," *Thin Shell Structure: Theory, Experiment and Design*, edited by Y. C. Fung and E. E. Sechler, Prentice-Hall, Englewood Cliffs, NJ, 1974, pp. 435–452.

[12]Kapania, R. K. and Yang, T. Y., "Formulation of an Imperfect Quadrilateral Doubly Curved Shell Element for Postbuckling Analysis," *AIAA Journal*, Vol. 24, Feb. 1986, pp. 310–311.

[13]Saigal, S., Yang, T. Y., and Kapania, R. K., "Dynamic Buckling of Imperfection-Sensitive Shell Structures," *Proceedings of the AIAA/ASME/ASCE/AHS 27th Structures, Structural Dynamics, and Material Conference*, May 1986, AIAA, NY, pp. 569–575.

[14]Budiansky, B. and Roth, R. S., "Axisymmetric Dynamic Buckling of Clamped Shallow Spherical Shells," NASA TN D-1510, 1962, pp. 597–606.

[15]Huang, N. C., "Axisymmetric Dynamic Snap-Through of Elastic Clamped Shallow Spherical Shells," *AIAA Journal*, Vol. 7, Feb. 1979, pp. 215–220.

[16]Stricklin, J. A., Martinez, J. E., Tillerson, J. R., Hong, J. H., and Haisler, W. E., "Nonlinear Dynamic Analysis of Shells of Revolution by Matrix Displacement Method," *AIAA Journal*, Vol. 9, April 1971, pp. 629–636.

[17]Kao, R. and Perrone, N., "Dynamic Buckling of Axisymmetric Spherical Caps with Initial Imperfections," *Computers and Structures*, Vol. 9, 1978, pp. 463–473.

[18]Kao, R., "Nonlinear Dynamic Buckling of Spherical Caps with Initial Imperfections," *Computers and Structures*, Vol. 12, 1980, pp. 49–63.

[19]Ishizaki, T. and Bathe, K. J., "On the Finite Element Large Displacement and Elastic-Plastic Dynamic Analysis of Shell Structures," *Computers and Structures*, Vol. 12, 1980, pp. 309–318.

[20]Niordson, F. I., *Shell Theory*, North-Holland Series in Applied Mechanics, the Netherlands, 1985.

[21]Clough, R. W. and Penzien, J., *Dynamics of Structures*, McGraw-Hill, New York, 1975, pp. 194–198.

[22]Yang, T. Y. and Saigal, S., "A Curved Quadrilateral Element for Static Analysis of Shells with Geometric and Material Nonlinearities," *International Journal for Numerical Methods in Engineering*, Vol. 21, 1985, pp. 617–635.

[23]Zienkiewicz, O. C., *The Finite Element Method*, 3rd ed., McGraw-Hill, London, 1977.

[24]Owen, D. R. J. and Hinton, E., *Finite Elements in Plasticity: Theory and Practice*, Pineridge Press, Swansea, England, 1980.